APPLIED TRANSONICS AT GRUMMAN

W. H. Davis
Grumman Aircraft Systems
Bethpage, NY

ABSTRACT

A review of several applications of Computational Fluid Dynamics (CFD) to various aspects of aerodynamic design recently carried out at Grumman is presented. The emphasis is placed on project-oriented applications where the ease of use of the methods and short start-to-completion times are required. Applications cover transonic wing design/optimization, wing mounted stores load prediction, transonic buffet alleviation, fuselage loads estimation, and compact offset diffuser design for advanced aircraft configurations. Computational methods employed include extended transonic small disturbance (automatic grid embedding) formulation for analysis/design/optimization and a thin layer Navier-Stokes formulation for both external and internal flow analyses.

INTRODUCTION

The major drivers for the application of transonic CFD at Grumman are the engineering projects, either in direct support of an in-production aircraft or its upgrade, or in the advanced development world. This type of project-oriented application puts a premium on aspects of the CFD method not necessarily associated only with accuracy. While accuracy is of course important, the ability to respond in a time frame of days is usually critical. No matter how advanced a computational capability might be, if it requires two weeks to set up the geometry and computational grid, and another two weeks to obtain useful numerical results, then that capability is useless to the project if, for example, answers are required in two days to support an on-going flight test. This reality has led to a concentration, for transonic flows, on two computational formulations: transonic small disturbance (TSD) for complex configurations, and judicious use of thin-layer Navier-Stokes (TLNS) for complex flow/single component analyses.

The utility of such an approach is attested to by the broad range of engineering problems to which CFD has been applied at Grumman. Among these applications are developing contours for wing design, aiding in aircraft component integration, providing aerodynamic predictions for other disciplines, and as a diagnostic tool to aid in wind tunnel or flight testing (see also ref. 1,2). The intent of this paper is to demonstrate that wide range of application.

CFD codes employing the extended 3-D TSD formulation play a major role in external aerodynamic design/analysis at Grumman. The benefits are many. They include the ability to analyze complex realistic aircraft plus component configurations while requiring only short set up times (automatic grid generation). The low computer memory demand (less than 2 MW) and short computational times (under 5 minutes: CRAY XMP 1.4) allow many sequential runs to be turned around in a single day making them ideal for the demanding time constraints of project work. Finally, high confidence in code accuracy comes from 10 years of continuing development work and hundreds of test case comparisons with data.

The NASA-Grumman Wing Body Code (TSD formulation) has progressed from the work of Boppe (ref. 3,4) to extensions by Aidala (ref. 5) to include canards, and the more recent work of Rosen (ref. 6,7,8) to handle wing mounted stores (multiple fin capability) while employing a rotated finite difference scheme for added robustness. Short computational times also have allowed the development, under contract to NASA Langley Research Center, of an optimization/design version of the code, TRO-3D (ref. 9,10), based on Aidala's original work (ref. 5). Optimization by maximizing drag polar efficiency while holding both aerodynamic (lift, moment) and geometric constraints is available. Wing design is also on option by minimizing differences in computed and specified target pressure distributions while maintaining geometric constraints. The optimization module controls both geometry modification and aerodynamic analysis module. The key feature that distinguishes this method from others is the use of aero-function shapes rather than arbitrary functions for geometry modification during the optimization process.

Use of design variables having specific aerodynamic origins has two major benefits. It reduces the computational time for optimization by requiring fewer design variables than for previous schemes and results in pressures that would be more acceptable to an aerodynamicist. Neither of these effects would be expected with an arbitrary set of polynomial bumps used as design variables.

Design variable shapes having an aerodynamic origin were developed from both 2-D and 3-D codes (ref. 11,12). The inverse code translates the aerodynamic input (a pressure change) into a geometric shape perturbation (a geometry change). The 2-D inverse code provides efficient, reliable results with a grid density that can resolve the necessary geometric detail. A 3-D inverse code provides spanwise shape functions to be used with the wing-section shape functions. This approach allows the strengths of the inverse and otpimization approaches to be combined. Design variable shapes having specific geometric origins were also developed. These include a leading edge nose radius shape and sets of shapes for leading and trailing edge camber used to model wing device deflections and shapes.

There is presently a catalogue of 25 aero-function shapes available (ref. 10). Not all of these shapes are required for every optimization case, and, in fact, as few as four shapes (design variables) can produce excellent results. One strength of these shapes is that their selection (or elimination) process becomes straightforward because the shapes produce

specific aerodynamic or geometric effects. Similarly, defining and enforcing geometric limits on the amount of additional wing thickness, twist camber device deflection, nose radius, etc. allowable in the final design is easily done as side constraints on the design variables rather than as constraint functions within the optimization algorithm. Full advantage of this last capability was taken during the following exercise.

A Natural Laminar Flow (NLF) Program sponsored jointly by NASA LaRC and NASA Ames-Dryden was initiated in 1984. A variable sweep transition flight test was proposed using the F-14 aircraft. NLF was to be attained by making changes to the baseline wing contours on the upper surface and outboard of the wing pivot point (fig. 1). Shape changes were to be affected by adding a foam and fiberglass glove over the wing in this region. These geometry changes were limited not only in extent but also to being volume-added-only; no cutting of the original wing contour was allowed. It was thought that the level flight condition at $M_\infty = 0.7$, $C_L = 0.4$, altitude = 30,000 ft and wing sweep of 20 deg. would be particularily troublesome since the baseline pressure distribution in no way resembled the classic long chord run plateaus known to produce NLF. It was felt that the TRO-3D code, in the pressure design mode, could be applied in this case to determine if it was physically possible to attain NLF-type pressure distributions within these geometric constraints (ref. 13).

Two target pressure distributions were selected which were known to support laminar flow to 55 and 65 precent chord from 2-D tests and were applied, for each case, at three stations spanning the wing. Six design variables were chosen: angle of attack, inboard and outboard camber shapes developed specifically for 3-D root and tip effects, inboard and outboard chordwise load shift shapes developed from the 2-D inverse code, and a leading edge incremental radius shape. All shape changes were constrained to be positive (volume added) and to act only on the upper wing surface outboard of the glove. Four optimization cycles and a total of 38 calls to the analysis code were required. Detailed descriptions of all shape functions and their development are given in reference 10.

Results of both design cases are shown in Figures 2 and 3. Excellent agreement with target pressures are obtained in both cases considering that the targets were selected with no a priori knowledge that a unique geometry (meeting the particular design requirements) existed. Figure 4 shows airfoil geometries at three span stations for both cases. Thus, NLF type pressure distributions can be attained at this flight condition while maintaining the strict geometric constraints. Given the original F-14 wing/body geometry set which already existed, the total time required to complete this preliminary stage of the wing design was two days. NASA LaRC personnel continued refinement of the wing design using both 2-D and 3-D methods, in particular to take into account aerodynamic performance at off design flight conditions and to reduce added thickness in the trailing edge flap hinge region at 75% chord.

TRANSONIC STORES LOADS PREDICTION

The latest extension to the NASA-Grumman Transonic Wing-Body Code, funded by a contract through NASA Langley Research Center, includes the additional capability to handle isolated or under wing, pylon mounted stores with multiple fore and aft fins (ref. 8). The use of a 5-level embedded grid approach ending in a fine, body-fitted store C-grid and employing exact body boundary conditions, yields accurate store loads prediction and

store/configuration interaction effects. The incorporation of a rotated finite difference scheme in all grids substantially increases robustness allowing more accurate treatment of low aspect ratio, highly swept and tapered wings. Supersonic farfield boundary conditions also allow for a limited supersonic freestream capability. All grid generation and interaction is done automatically.

The aerodynamic prediction capability of the code for isolated stores is demonstrated in figure 5 for the GBU-15 configuration (ref. 14). Both absolute levels of lift and moment through the full configuration component build-up, are accurately calculated. The store body results include viscous crossflow estimates. A more complicated geometry, the Nielson wing body/pylon/store configuration (ref. 15) is shown in figure 6. The strong wing-store interaction effects evident in the store pressures (fig. 7) are accurately predicted by the code. This latest version of NASA-Grumman Transonic Wing-Body Code will be relied upon heavily for a large percentage of external aerodynamic CFD design/analysis applications at Grumman.

F-14A$^+$ TRANSONIC BUFFET

The first stage of a major F-14A upgrade to an F-14D (engine plus avionics) required changes to incorporate the F110-GE-400 engine. This version, designated F-14A$^+$, required aft-end nacelle contour modifications, including the fuselage sponson fairings, and the interfairing between the pancake centerbody and the nozzle (figure 8) to accept the new engine. These contour modifications were completed during wind tunnel testing in April 1985. The new engine also had modified shapes for the nozzle flap and forward composite regions.

During initial flight testing of the full scale development aircraft, the pilot reported the appearance of buffet at transonic conditions, in particular M_∞=0.8-1.0 at 7500 feet altitude. This flight condition is encountered only transiently during acceleration, thus the buffet was not considered a major problem. Nevertheless, an effort was made to understand the causes of the buffet and suggest methods to possibly alleviate it.

Subsequent flight testing uncovered several pertinent pieces of information about the buffet. The frequency of motion induced at the pilot seat was seven Hertz, corresponding to the fuselage first bending moment. The buffet was alleviated by two in-flight configuration changes: opening the nozzle flaps to the max A/B position and cracking open (10° deflection) the speed brake (located on the aft region of the pancake). It is also interesting to note that the aft pancake shape of the production F-14A was actually modified during its initial development to alleviate a very early buffet problem. The F-14A production pancake shows this effect as trailing edge notches on either side of the centerbody.

Several mechanisms were suspected as the cause of the buffet, and each gave rise to a plan of investigation. For the purpose of this paper we concentrate on one such area: possible strong shock/boundary layer interaction in the aft-end region due to the configuration changes. A general picture of the complex 3-D aft-end flowfield was sought using CFD. The hope was to predict if and where strong shocks, leading to possible flow separation and buffet, might be occuring. Also the predicted effect of max A/B nozzle and brake deflection configuration changes on the shock pattern and strength

should not be inconsistent with the flight tests; i.e., both changes alleviated the buffet (in this case presumeably by weakening the shocks).

The 3-D TSD code with pylon mounted stores capability, described in the previous section, was used to investigate the effects of the nacelles, pancake and nozzles, see figure 9. Actual nacelle lines were converted into equivalent axisymmetric shapes for modeling in the body conforming stores portion of the code. Centerbodies for both the pre-production and production F-14A pancake were modeled as a pylon with the wing acting as a symmetry plane. A freestream Mach number of 0.93 was selected for the analysis. Figures 10, 11 and 12 show planform views of the analytically predicted shock patterns. In figure 10, the F-14A cruise (nozzle flaps in the cruise position) with the pre-production pancake (top of figure) shows a strong shock at station 800. The production pancake (bottom of figure) sweeps the shock, weakening it, and removes area after the shock. Both effects may have contributed to the ability of the production pancake to reduce the F-14A pre-production buffet. Figure 11 shows that the F-14A$^+$ cruise shape throws a strong shock at the center of the pancake at station 750, which is not there for the F-14A cruise. The opening of the speed brake for the F-14A$^+$ cruise, figure 12, shows that the shock at station 750 goes away. In the same figure, the opening of the F-14A$^+$ nozzle flaps to the max A/B position has an even more dramatic effect in that all pancake and nozzle shocks are removed.

The TSD code for this case should not be expected to predict exact shock positions since the model is geometrically approximate. But general trends can be used diagnostically. The TSD calculations show that the appearance and disappearance (or weakening) of the shocks with various configuration changes, i.e., opening the nozzle to max A/B or cracking open the speed brake, correspond to the appearance and disappearance of the buffet from flight test results. This suggests that a strong nacelle/pancake shock around the 750 fuselage station may be the cause of the aft-end buffet through unstable shock induced flow separation.

This being the case, then the buffet might be reduced by stabilizing the shock (or reducing its strength). Vortex generators placed forward of the shock, energizing the boundary layer, would tend to stabilize the shock by reducing the tendency for shock induced flow separation. Generally, though, a complete alleviation of buffet by this means would not be expected. As flight Mach number, and thus shock strength, continues to increase, shock induced flow separation would again dominate the flow, overiding the beneficial boundary layer energizing effects of the vortex generators. Thus a delay of buffet onset is most reasonably to be expected if the vortex generators are at all effective.

Previous, low speed, wind tunnel tests at Grumman had shown that the counter-rotating vortex generator configuration was the most effective and had a downstream effective length of approximately 30 inches. Thus to affect the shock patterns of the F-14A$^+$ with the cruise nozzle flaps shown in the lower portion of figure 11, two rows of counter-rotating vortex generators were attached to the upper surface pancake region and continued onto the inner portion of the nacelle. These rows were placed at positions just forward of the predicted shock locations. The forward row was placed at fuselage station 740 and the aft row at fuselage station 770.

Subsequent flight tests showed that these vortex generators did indeed affect the buffet levels as anticipated. Figure 13 shows a plot of flight test results of maximum peak-to-peak g's (measured at the pilots seat) for the aircraft as Mach number is increased. The vortex generators have reduced F-

14A$^+$ buffet levels to those of the F-14A except at the higher Mach numbers. In fact, if a level of 0.2 g's is taken as reference for buffet onset, this boundary for the F-14A$^+$ at Mach 0.75 was pushed to Mach 0.88. This is still not quite at the F-14A level of Mach 0.95, but is a substantial improvement.

THIN LAYER NAVIER-STOKES

The CFD methods discussed so far offer powerful tools to the designer as long as the flow remains attached, but future requirements and constraints are emerging which force the designer into dealing with, at times, very large regions of flow separation. External vortices generated by sharp forebody chines or wing leading edges can produce dominant aerodynamic forces. While vortex formation at sharp edges and subsequent convection through the flowfield may be approached with the Euler formulation (this avenue is also being studied at Grumman, see references 16, 17, and 18), flow separation from smooth surfaces such as wings at high loading levels and forebodies at high angles of attack can have profound effects on aerodynamic performance.

Internal designs for inlets and nozzles can experience even more difficulty in this area. New aircraft configurations are forcing the use of highly offset compact diffusers which may exhibit flow separation and strong secondary flows leading to large total pressure losses and distortion. Prediction of these losses during the design process is critical to engine and aircraft performance.

Strong viscous effects with large total pressure losses can be simulated only with some form of the Navier-Stokes equations. Grumman has been working with the time-dependent three-dimensional thin-layer Navier-Stokes (TLNS) code ARC3D (ref.19) developed at NASA Ames Research Center. ARC3D is based on the Beam and Warming implicit approximate factorization algorithm and is a central difference 2nd order accurate, fully conservative finite difference code employing the Baldwin-Lomax turbulence model. Various single grid topologies have been explored for external flow over arbitrary forebodies and wings and for internal duct flows. Grids are all constructed using the transfinite interpolation method (ref. 20). An efficient code for generating such grids has been developed by B. Wedan of NASA Langley Research Center and forms the basis of our grid generation codes, both external and internal.

Unfortunately, accurate full configuration TLNS analysis on a routine basis for design purposes is not yet realizable because of grid size limitations and very large CPU times. But single component analyses using up to 120,000 points and requiring about one hour CPU time on a CRAY XMP 1.4 have shown quite good results in many cases and can be used sparingly in critical design situations. A growing set of favorable comparisons of analysis with data for forebody, wing, and internal flows is helping to develop confidence in ARC3D as a robust and reliable design/analysis tool. The following cases are examples of using the TLNS code to aid in design work.

FUSELAGE LOADS ESTIMATION

During an aircraft configuration development or modification, a Master Maneuver Program (MMP), developed at Grumman, is used to determine aircraft component loads. Control surface deflections, control laws, and wind tunnel

aerodynamic data, along with component flexibilities are used to fly the configuration through the time histories of multiple maneuvers. The result is a series of time histories of component loads.

MMP prediction of fuselage loadings, particularly during sideslip maneuvers, depends upon establishing side force distributions at a variety of flight conditions. Generally, due to limited wind tunnel data (i.e. total forces), these distributions are estimated. For example, one side force distribution for the A-6A had been approximated by scaling a baseline triangular distribution to match total side force and adjusted by adding a sine wave couple to correctly place the center of pressure as determined from wind tunnel total forces. This baseline triangular distribution had been constructed for Mach 1.07, 3.3° angle of attack, and 4.9° sideslip (rolling pullout maneuver).

In keeping with advances in CFD, a general cooperative effort between the Aerodynamics and Loads sections at Grumman has begun to look at the possibility of using CFD to augment loads estimation methodology. The A-6F, being a recent design effort, was taken as one focal point. The A-6F configuration is an evolutionary development of the in-production A-6E. The A-6F includes updated avionics and advanced engine for improved aircraft performance. Specifically, the transonic side force distribution was investigated since, again, limited wind tunnel data would require a dependence on estimating procedures. The ability of advanced CFD methods to match wind tunnel data and validate the estimated baseline triangular distribution was of particular interest.

The first attempt to estimate the fuselage side force distribution was made with VSAERO (ref. 21). This allowed wing/body configuration analysis in sideslip (fig. 14). Unfortunately, viscous effects, which can play a major role in slender body forces at angle of attack are only weakly modeled, and the limitation to subsonic flow restricted the usefulness of VSAERO. Since no experimental load distributions were available, the analytic results were compared to wind tunnel (wing/body model) total forces, moments and center of pressure location. Even in the low speed cases, the VSAERO calculations placed the center of pressure far forward of the experimental data even after making allowances for viscous crossflow effects. This is consistent with an under-estimation of visous effects.

To more accurately assess these viscous effects, the TLNS code was used to analyze the A-6F body alone geometry. Since side forces at relatively low angle of attack were sought, wing effects were not considered crucial at this point. This approach would also allow the full Mach range of interest to be covered. The complete cycle, pre-processing/analysis/post-processing for the TLNS calculations, was completed within two days. Full 3-D grids were generated over the A-6F fuselage using the transfinite interpolator and a "QUICK" surface model (ref. 3) for the configuration (fig. 15) with inlets faired over. The grid contained 96,000 points, 60 axial (clustered to the nose), 40 circumferential, and 40 radial (clustered normal to the surface). Each calculation required 40 minutes of CPU time on a CRAY XMP 1.4 to reduce the L2 residual (ref. 17) three orders of magnitude.

Comparisons to wind tunnel data in figures 16 and 17 for total forces in sideslip give some confidence that the TLNS analytic results are believable. Figure 16 shows the beta (sideslip) derivative of side force plotted over the transonic Mach range. At low speeds both VSAERO and TLNS slightly overpredict the wing/body side force derivative ($C_{y\beta}$). The lack of a wing in the TLNS model does not seem to be critical to this side force calculation. At higher

speeds VSAERO actually predicts an increasing derivative, probably due to the combination of the subsonic limitation and weak viscous effects, while the TLNS more correctly follows the wind tunnel test trend of decreasing derivative with Mach number. The TLNS Code's over-prediction of this derivative may be due to an insufficient number of grid points for the calculation. At Mach 1.07 the expected decrement due to angle of attack is correctly predicted. Figure 17 shows the beta derivative of the yawing moment plotted over the transonic range. Both VSAERO and TLNS do quite well in reproducing the wind tunnel results. Finally, in all cases, the VSAERO predictions place the center of pressure of the fuselage side forces well ahead of the nose while the TLNS code correctly follows the wind tunnel results by placing the center of pressure consistently just slightly aft of the fuselage nose.

Confident now that in terms of total side forces and moments, VSAERO and the TLNS codes are accurate at low speeds and the TLNS code is consistent with data in the transonic regime, the side force distribution can now be examined. Figure 18 compares both VSAERO and TLNS estimates to the original baseline triangular distribution. Note that both TLNS and triangular distribution are for full flight conditions, while VSAERO estimates are for reduced Mach number. Three points can be made. First, as might be expected, all distributions are in general agreement showing a forward concentration of side load. Second, both VSAERO and TLNS distributions show higher forward loadings and somewhat steeper gradients than the triangular estimate. Third, the larger, more aft loading of TLNS compared to VSAERO is expected due to the higher Mach number used for the TLNS calculation. It remains to corroborate these differences with wind tunnel testing and to understand their signifigance with respect to component loading. But these preliminary results indicate that advanced CFD methods can be useful in enhancing transonic loads estimating methodology.

COMPACT/OFFSET DIFFUSER

Highly offset, compact diffusers for advanced aircraft propulsion systems offer several advantages. These tightly packaged systems offer lightweight, low volume designs. They do have their disadvantages though. Large secondary flows including separation can lead to excessive total pressure distortions at the engine face and possibly engine stall. Limited experimental work and a need for a basic understanding of the physical phenomena, as applied to design methodology, prompted an internally funded program in this area within the Propulsion Section at Grumman (ref. 22). Experimental work was aimed at extending the compact diffuser data base and providing a relevant focal point for CFD calculations.

The offset diffuser test configuration is shown in figure 19. The basic diffuser design has a rectangular inlet transitioning to a circular engine face including a central compressor bullet. An offset of 50% of axial length is applied in one plane only. Forty total pressure probes cover the exit plane with a moveable rake of probes employed at various axial stations along the duct to determine losses near the wall. Static pressure ports were stationed from inlet to exit along top and bottom centerline. A removeable wall section was designed to accommodate various boundary layer control (BLC) devices including suction, blowing, and vortex generators. The test rig was back-pressured to yield a range of inlet flow conditions; of particular interest here is a throat (inlet) Mach number of 0.72.

Preliminary estimates of surface static pressures, separation location, and BLC mass flow to alleviate flow separation were made using the VSAERO Code and details can be found in ref. 22. Of particular interest here is the use of the TLNS Code to predict total pressure losses, engine face distortion, and to give us a better understanding of the role of separation and secondary flows in the loss process. The surface grid for the computational model is shown in figure 20. The 3-D grid, generated by transfinite interpolation, is a symmetric O-H topology containing 112,000 points with a centerline collapsed singularity surface. The grid is clustered axially towards the engine face and radially towards the wall where grid orthogonality is maintained.

The symmetry plane velocity vector plot in figure 21 shows lower surface flow separation occuring at about 40% down the duct length (enlarged portion at left of the figure), very close to the test results, and, in fact, the VSAERO prediction. The upper surface centerline (enlarged portion at right of the figure) shows a thickening of the boundary layer but no separation. VSAERO predicts flow separation at this point. Test results are inconclusive as to the appearance of flow separation here but do show large total pressure losses (9%) in this region, which the TLNS calculation, as will be shown later, quite nicely corroborates.

Figure 22 shows crossflow velocities indicating that at approximately 60% down the duct the initial formation of a vortex appears in the lower quadrant. This vortex is probably driven by the three-dimensional flow separation which had occurred just upstream as shown in the previous figure. This vortex intensifies and is driven further down into the lower quadrant as the exit plane is approached. The development of the total pressure profile normal to the lower wall, as we move down the duct, is shown in the lower part of figure 22. Agreement is fair, with the poorest comparison near the wall. The data show a maximum total pressure loss of approximately 25% near the wall at station D. As we move downstream to the exit at station F, the total pressure has actually recovered approximately 38% of the maximum loss which occurred at the upstream station D. This is most probably due to mixing from the vortex in this region. The TLNS calculation shows this beneficial mixing effect at the outer edge of this region but fails as we move closer to the wall. This is probably due to inadequate grid resolution in this critical region. The total pressure calculations at the exit plane between the bullet and the upper wall compare quite well to the data.

Figure 23 compares total pressure contours at the exit plane for the test data, on the left, and the TLNS calculation, on the right. The overall agreement is quite good, with the lower quadrant vortex position appearing slightly low, giving rise to an over-prediction of losses near the outer wall and an under-prediction near the center bullet. The upper region losses and pattern are accurately predicted. Figure 23 shows that calculated total pressure recovery (an area weighted average of exit total pressures referenced to the incoming total pressure) agrees very well with test data, and that max-min distortion values (the difference between maximum and minimum total pressures at a given plane referenced to the area weighted average at that plane) differ only by 2%.

CLOSING REMARKS

Advances in CFD algorithms along with computer size and speed have come at a fast pace in the past five years. This has made available a wide range of new tools to aid the engineer in either the design of new configurations or in understanding and diagnosing problem areas in current aircraft. The development of transonic methods, in particular, spans the range from transonic small disturbance to full potential, Euler and finally the Reynolds averaged form of the Navier-Stokes equations (generally in a thin-layer formulation). For design and diagnostic applications the engineering group at Grumman has concentrated efforts at both ends of that spectrum, TSD and TLNS. Using the TSD formulation, the setup and analysis of very complex configurations can be handled fast, a particularly important requirement within the real world of project-oriented tasks, and quite accurately. As long as flow separation does not dominate the aerodynamics, this will continue to be the favored approach.

For cases where strong viscous effects are dominant and may lead to flow separation, neither full potential nor Euler methods offer any advantage over TSD. In addition, the time consuming and not always straight forward process of generating a computational grid over very complex configurations, required for the higher order methods, can become prohibitive. The most effective approach is judicious use of the TLNS method. The reward, i.e., calculation of very complex flow fields, is a powerful incentive but is gained at some expense. Complex multiple component configurations cannot be handled, since even if a grid could be generated within a reasonable period of time, the huge number of grid points would result in prohibitive computational times and cost. But much valuable information for design or diagnosis can be obtained by using the TLNS method for selective component analysis, keeping setup and computational times down to a more cost effective level.

It would appear that this route ignores the middle of the CFD spectrum, but that is not entirely true. The Euler formulation is beginning to show promise for full configurations which aerodynamically rely on vortex formation from sharp leading edges for added performance. For this type of flow, the Euler method is probably superior to both TSD and TLNS. The irrotational TSD formulation precludes vortex formation, and Euler is much faster and less costly than TLNS. A major effort in this area is being carried on in the Grumman Research Department and will surely filter up to the engineering applications level as needs arise and validation cases mount up. But to date, the ends of the CFD spectrum, TSD and judicous use of TLNS, have proven quite useful.

ACKNOWLEDGEMENT

The author expresses his appreciation to the many individuals at Grumman whose efforts are included in this work: Bruce Rosen (TSD stores/F-14 buffet); James Capodieci, Ray Mangan and Dick Kita (F-14 buffet); Marty Bourbin (A-6F loads); Ron Tindell and Dr. Tom Alston (offset diffuser). A final recognition goes to Charles W. Boppe for general technical and editorial guidance.

REFERENCES

1. Boppe, C. W.: Computational Aerodynamic Design: X-29, Ths Gulfstream Series, and a Tactical Fighter. SAE Paper 851789, October 1985.

2. Boppe, C. W.: Elements of Computational Engine-Airframe Integration. Progress in Aeronautics, Volume 102, 1986.

3. Boppe, C. W.: Transonic Flow Field Analysis for Wing-Fuselage Configurations. NASA CR-3243, May 1980.

4. Boppe, C. W.: Aerodynamic Analysis for Aircraft with Nacelles, Pylons and Winglets at Transonic Speeds. NASA CR-4066, April 1987.

5. Aidala, P. V.: Numerical Aircraft Design Using 3-D Transonic Analysis with Optimization. Volume 2, Part 2: Fighter Design. AFWAL-TR-81-3091, Volume 2, Part 2, U.S. Air Force, August 1981.

6. Rosen B. S.: Computational Transonic Analysis of Canted Winglets. Journal of Aircraft, Volume 21, pp 873-878, November 1984.

7. Rosen, B. S.: Body Flow Field Simulation and Force/Moment Prediction at Transonic Speeds. AIAA Paper 85-0423, January 1985.

8. Rosen, B. S.: External Store Carriage Loads Prediction at Transonic Speeds. AIAA Paper 88-0003, January 1988.

9. Aidala, P. V., Davis, W. H., Mason, W. H.: Smart Aerodynamic Optimization. AIAA Paper 83-1863, July 1983.

10. Davis, W. H., Aidala, P. V., Mason, W. H.: A Study to Develop Improved Methods for the Design of Transonic Fighter Wings by the Use of Numerical Optimization. NASA-CR-3995, August 1986.

11. Davis, W. H.: TRO-2D: A Code for Rational Transonic Airfoil Design by Optimization. AIAA Paper 85-0425, January 1985.

12. Woodward, F. A.: Analysis and Design of Wing-Body Combinations at Subsonic and Supersonic Speeds. Journal of Aircraft, Volume 5, No. 6, November 1968.

13. Waggoner, E. G., Phillips, P. S., Viken, J. K., Davis, W. H.: Potential Flow Calculations and Preliminary Wing Design in Support of an NLF Variable Sweep Transition Flight Experiment. AIAA Paper 85-0426, January 1985.

14. Shadow, T. D.: Wind Tunnel Tests to Determine the Distributed Loads on a 0.25 Scale GBU-15 (CWW) Model at Transonic Mach Numbers. AEDC-TSR-80-P14, February 1980.

15. Stahara, S. S., Crisalli, A. J.: Data Report for a Test Program to Study Transonic Flow Fields about Wing-Body/Pylon/Store Combinations. AFOSR TR-79-1070, May 1978.

16. Melnik, R. E.: An Overview of Computational Fluid Dynamics Development and Application at Grumman. Presented at NASA Conference on Supercomputers in Aerospace, NASA Ames Research Center, Moffett Field, CA, March 10-12, 1987.

17. Volpe, G., Siclari, M. J., Jameson, A.: A New Multigrid Euler Method for Fighter-Type Configurations. AIAA Paper 87-1160-CP, June 1987.

18. Volpe, G., Siclari, M. J., Jameson, A.: Computation of Aircraft Flowfields by a Multigrid Euler Method. AIAA Paper 87-2268-CP, August 1987.

19. Pulliam, T., Steger, J.: Implicit Finite-Difference Simulations of 3-D Compressible Flow. AIAA Journal, Volume 18, No. 2, pp. 159-167, February 1980.

20. Eriksson, L. E.: Generation of Boundary-Conforming Grids Around Wing-Body Configurations Using Transfinite Interpolation. AIAA Journal, Volume 20, No. 10, pp 1313-1320, October 1982.

21. Maskew, B.: Prediction of Subsonic Aerodynamic Characteristics: A Case for Low-Order Panel Methods. Journal of Aircraft, Volume 19, No. 2, pp. 157-163, February 1982.

22. Tindell, R. H.: Highly Compact Inlet Diffuser Technology. AIAA Paper 87-1747, June 1987.

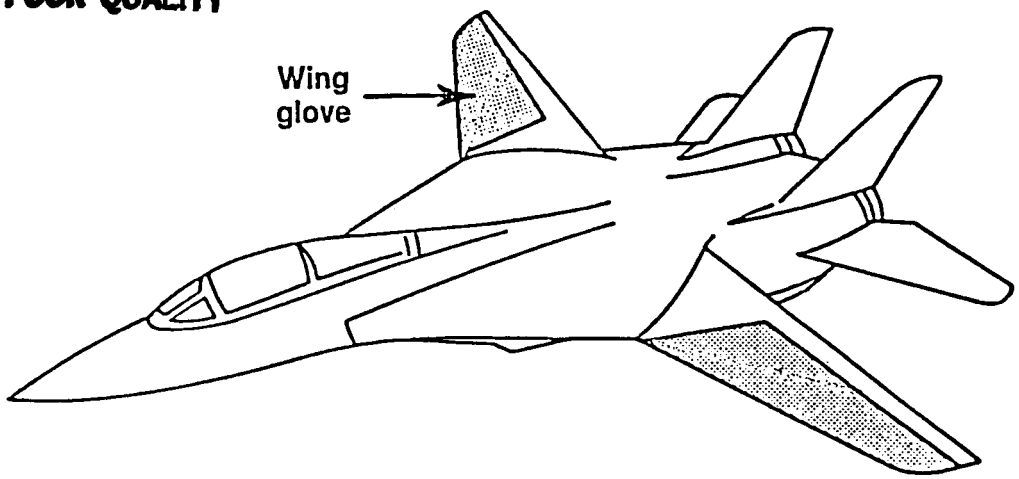

Figure 1. F-14/20° sweep configuration showing wing region available for NLF glove.

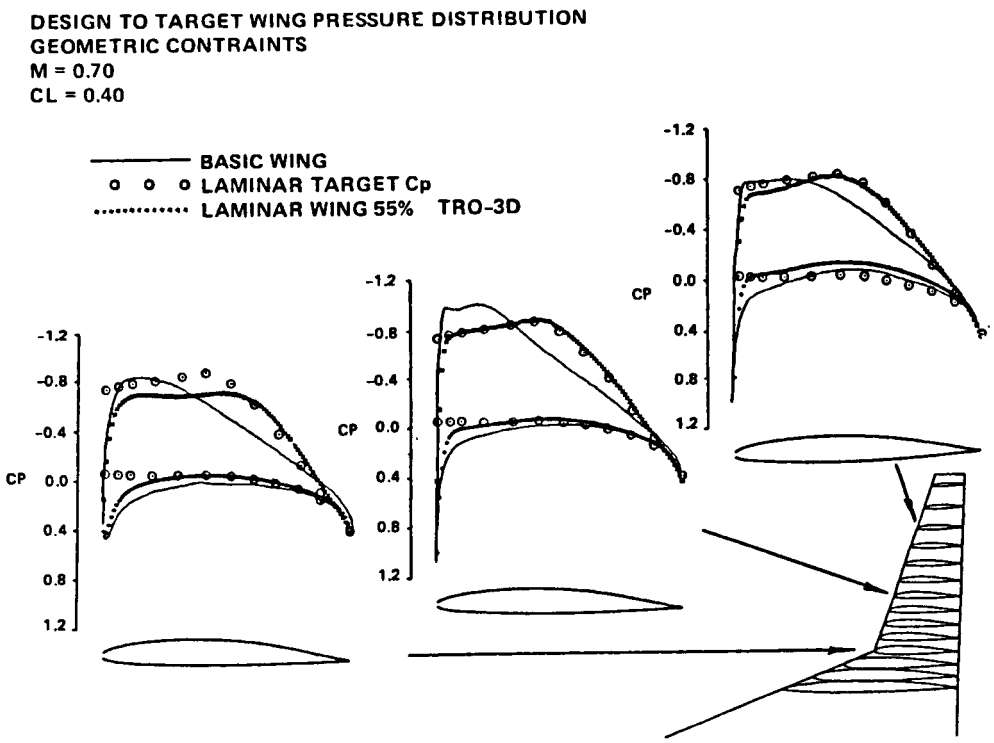

Figure 2. F-14/TRO-3D results for target pressure distribution with NLF to 55% chord.

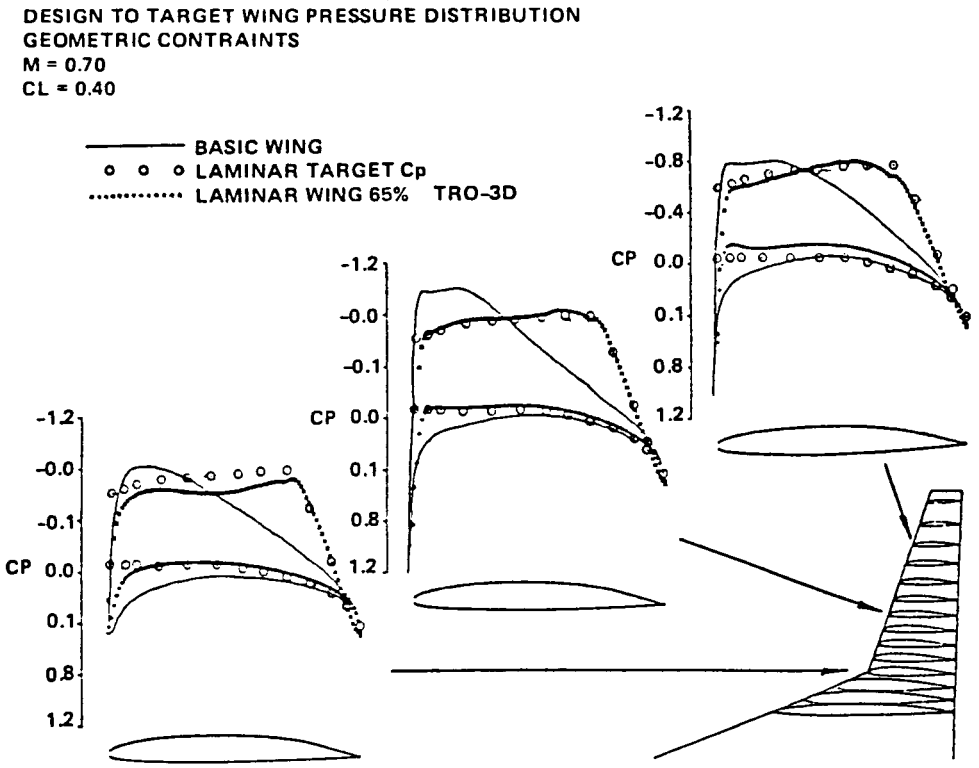

Figure 3. F-14/TRO-3D results for target pressure distribution with NLF to 65% chord.

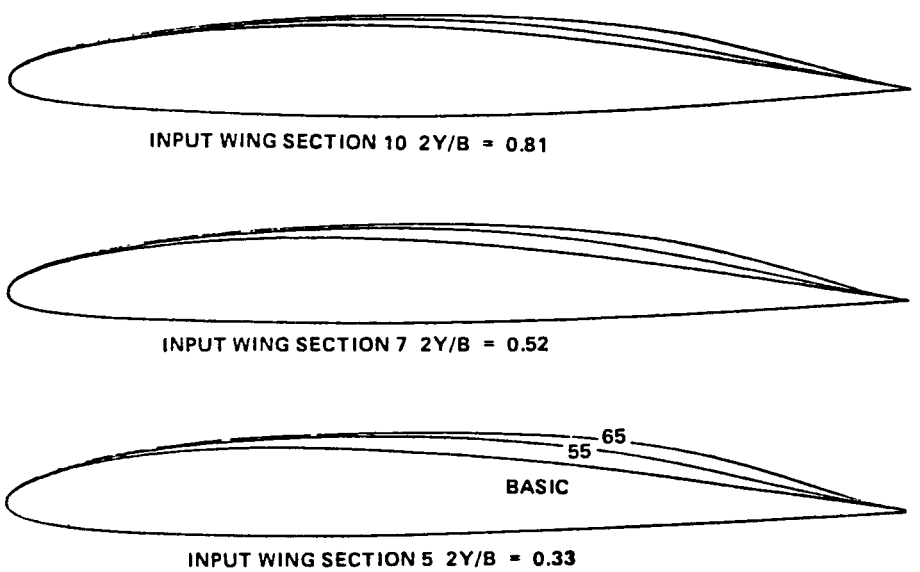

Figure 4. F-14/TRO-3D resulting airfoil shapes for NLF to both 55% and 65% chord.

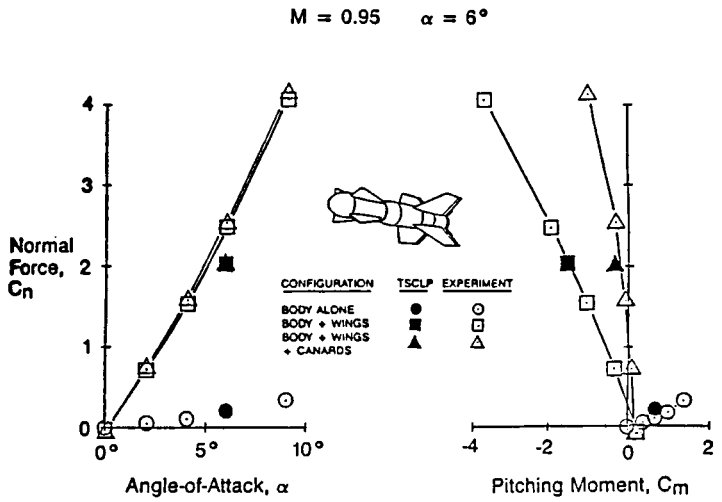

Figure 5. TSD: Force and moment correlation for GBU-15-CWW isolated store.

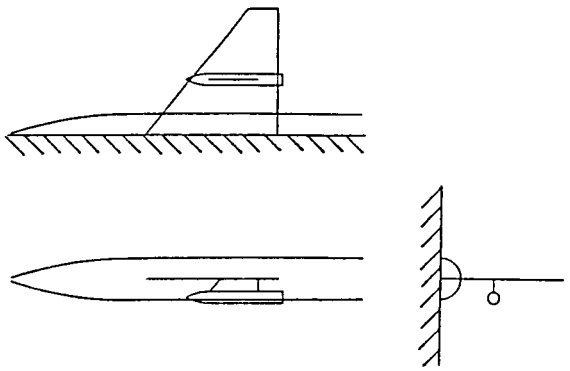

Figure 6. TSD: Geometry for Nielsen wing/fuselage/pylon/store.

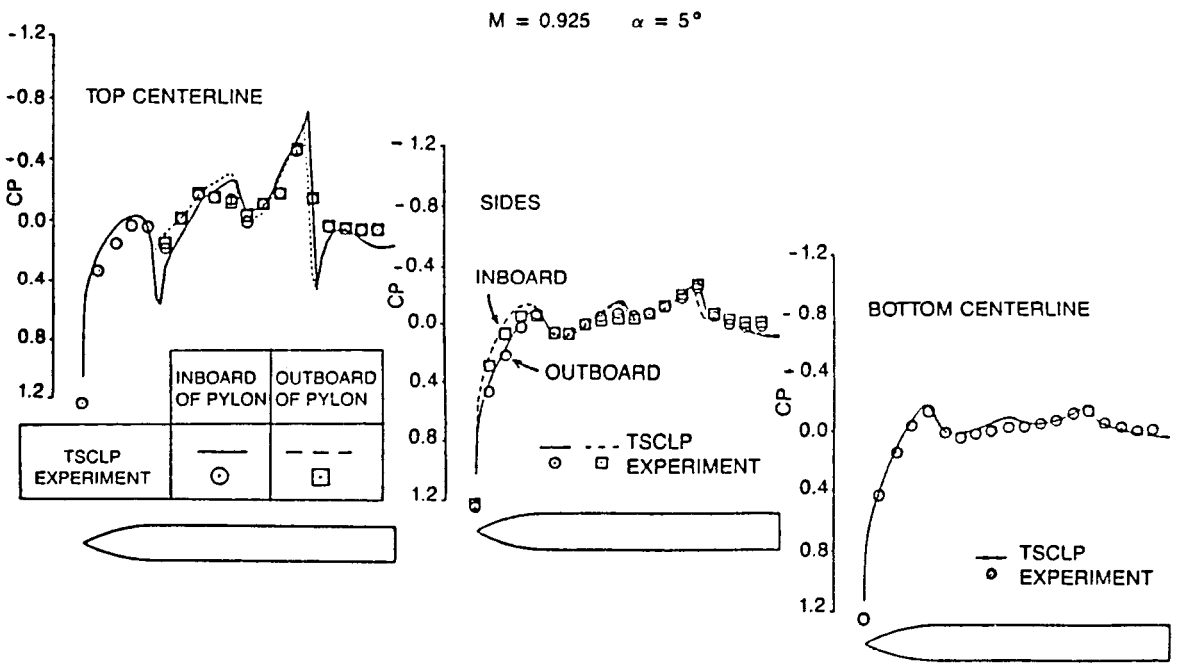

Figure 7. TSD: Store pressures for Nielsen wing/fuselage/pylon/store.

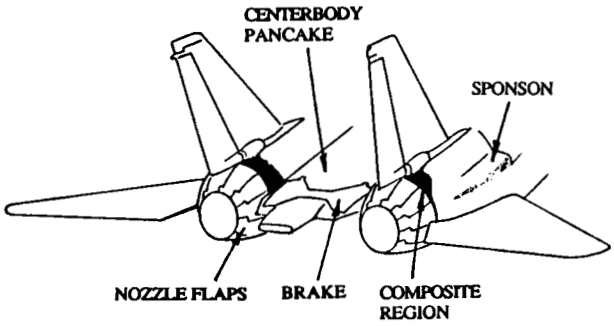

Figure 8. F-14A aft-end configuration.

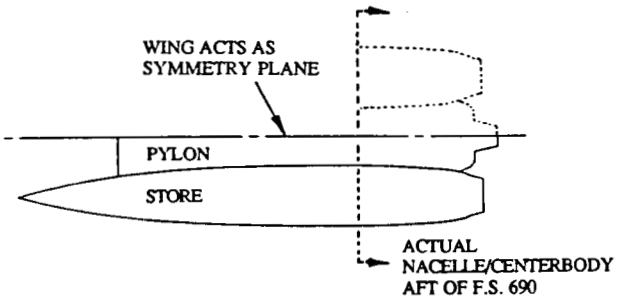

Figure 9. TSD model for F-14 aft-end buffet investigation.

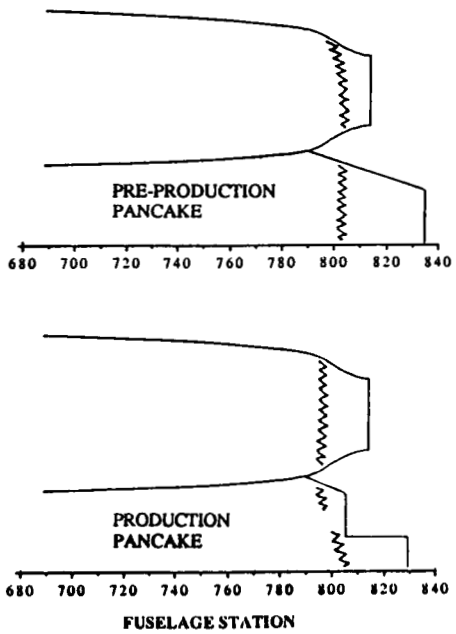

Figure 10. TSD predicted shock pattern. Effect of F-14A pre-production pancake modifications (cruise configuration at M_{∞}=0.93).

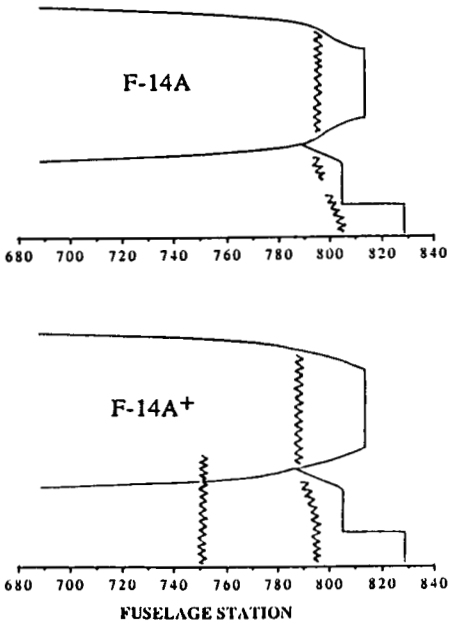

Figure 11. TSD predicted shock pattern. F-14A compared to F-14A^{+} (cruise configuration at M_{∞}=0.93).

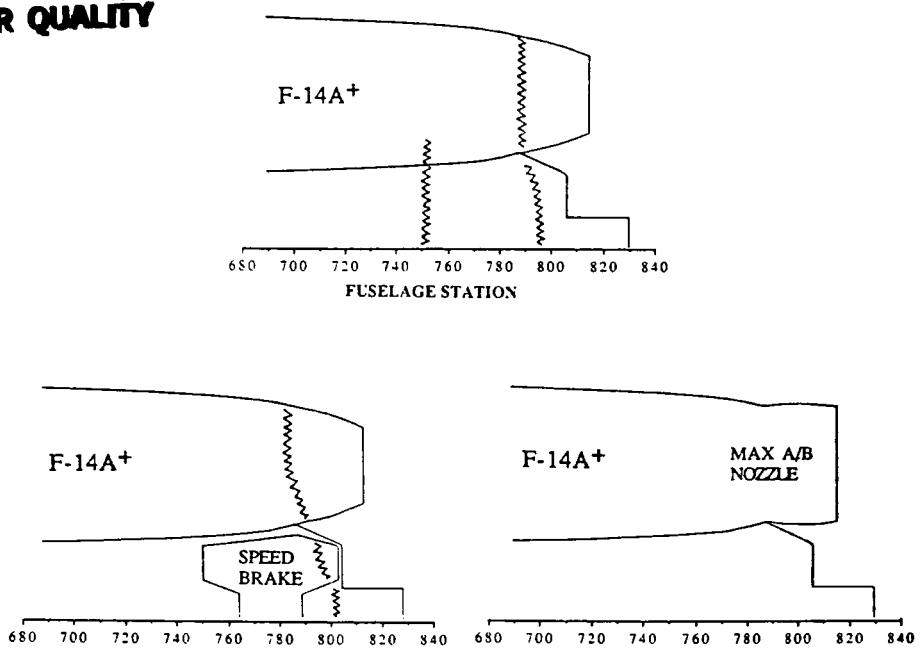

Figure 12. TSD predicted shock patterns. Effect of F-14A+ configuration changes at M_{∞}=0.93).

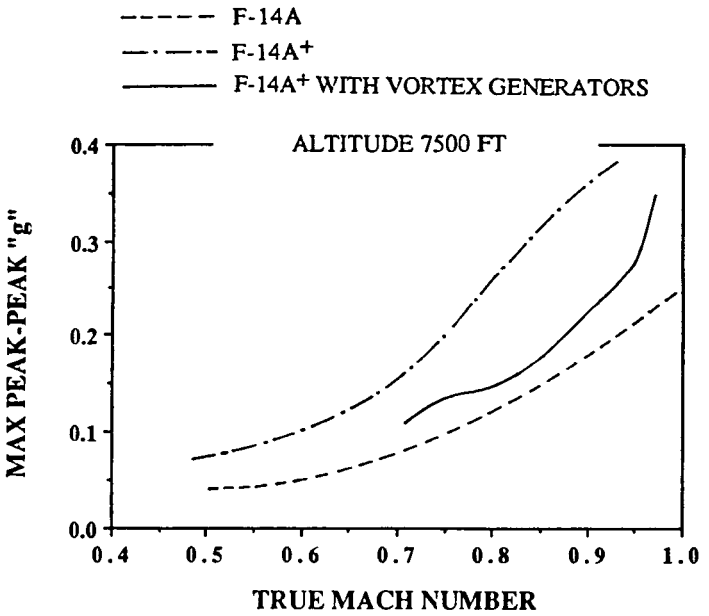

Figure 13. Flight test results. F-14A+ transonic buffet: effect of vortex generators added to upper surface pancake and nacelles at F.S. 740 and 770.

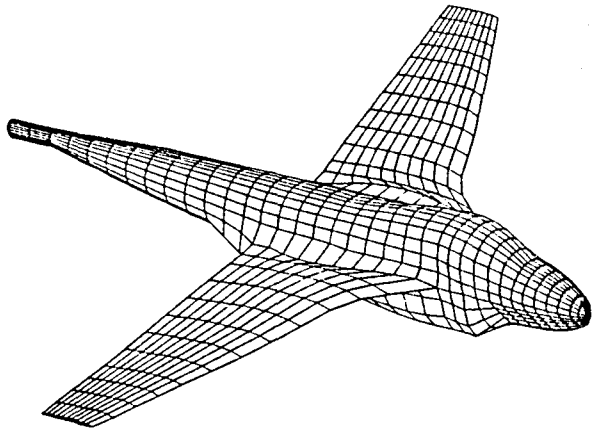

Figure 14. VSAERO panel model for A-6F side force distribution estimate.

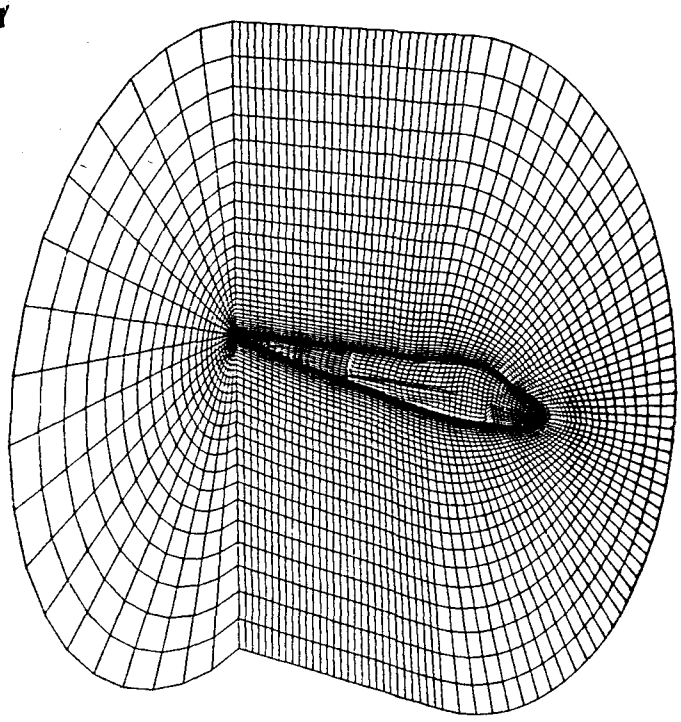

Figure 15. A-6F fuselage computational grid for TLNS calculation.

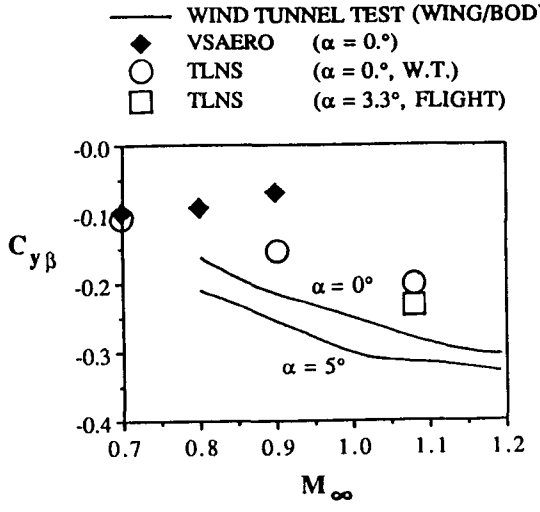

Figure 16. A-6F side force derivative in sideslip.

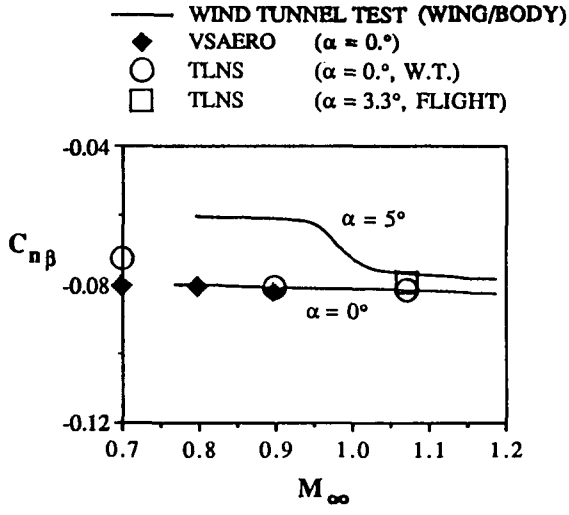

Figure 17. A-6F yawing moment derivative in sideslip.

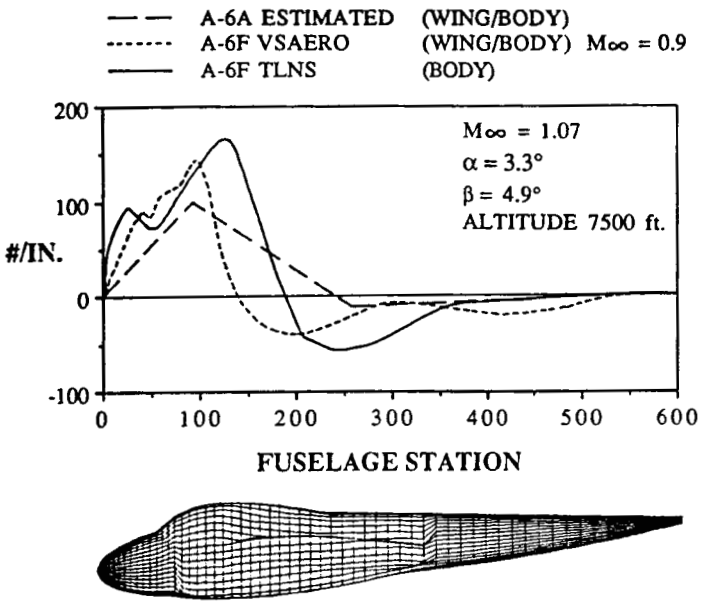

Figure 18. A-6F estimated side force distribution.

L	D	W	L/D	W/H	ΔY/L	A_2/A_1
22	10	9.2	2.2	2.0	0.50	1.89

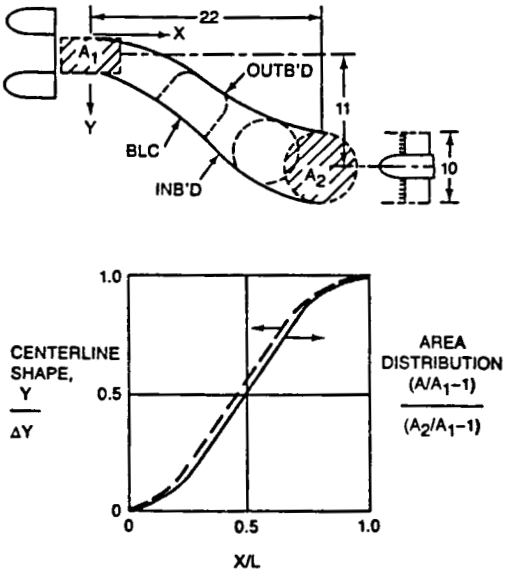

Figure 19. Offset diffuser test configuration definition.

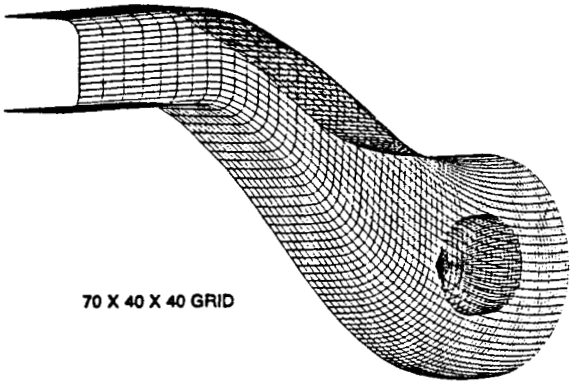

Figure 20. Offset diffuser computational surface grid for TLNS calculation.

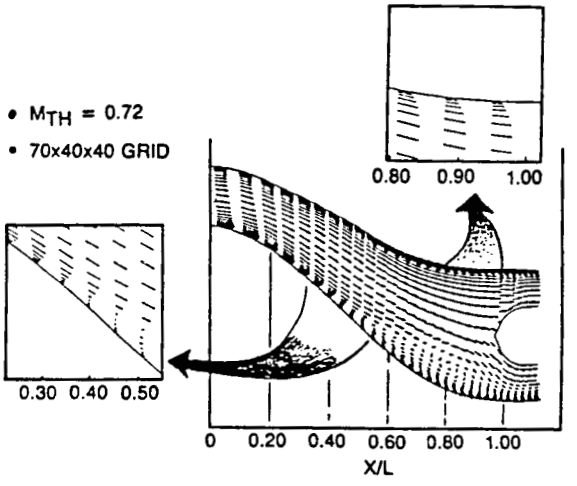

Figure 21. Offset diffuser symmetry plane velocity vectors from TLNS calculation.

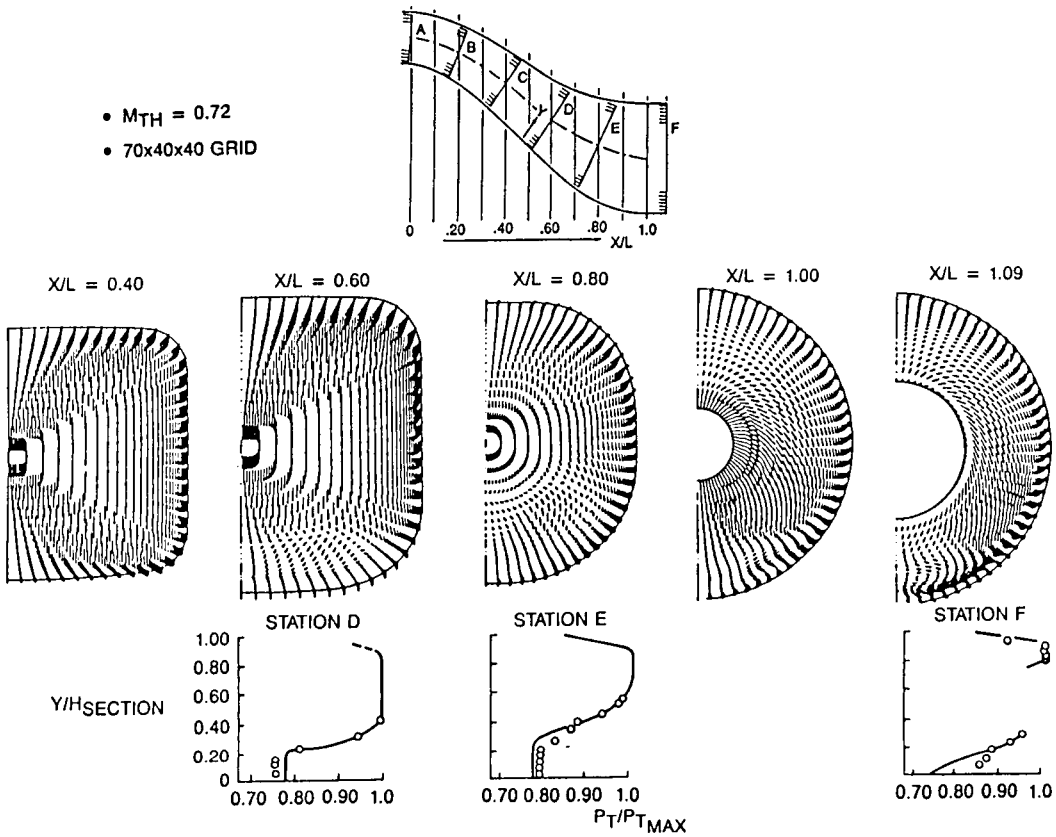

Figure 22. Offset diffuser cross-flow velocity vectors and wall total pressure losses, TLNS calculation compared to experimental data.

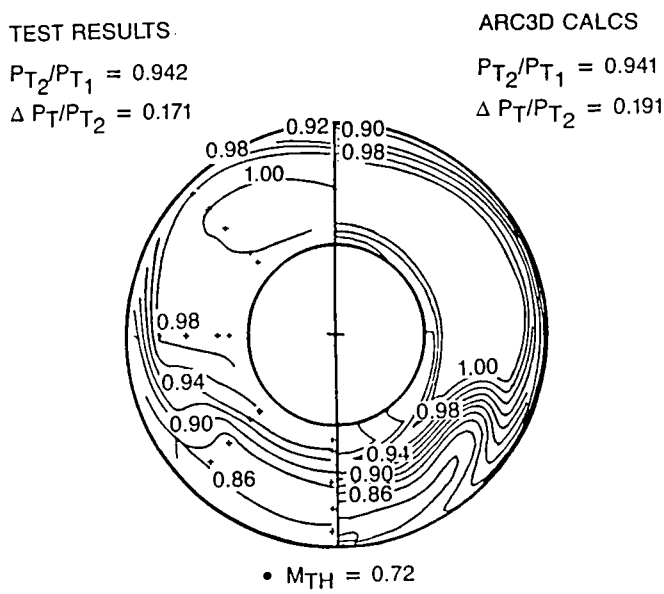

Figure 23. Offset diffuser exit total pressure profiles. TLNS calculation compared to experimental data.